EFFECT OF MANGANESE DOPING ON THE ELECTROCHEMICAL PERFORMANCE OF MOS_2 AS A CATHODE MATERIAL FOR RECHARGEABLE Zn-Ion BATTERIES

Huy Le-Quoc[1], Trang N.T.T[1], Duc Binh Luu[1], Thanh V. Hoang[1], Son L.V.T[2], Kien Nguyen-Ba[1]*, Anh T. Vo[1]*

[1]The University of Danang - University of Science and Technology, Vietnam
[2]The University of Danang - University of Science and Education, Vietnam

*Corresponding author: vtanh@dut.udn.vn, nbkien@dut.udn.vn

(Received: April 15, 2025; Revised: June 09, 2025; Accepted: June 18, 2025)

DOI: 10.31130/ud-jst.2025.23(9D).557E

Abstract - Aqueous zinc-ion batteries (AZIBs) show promise for grid-scale energy storage due to their intrinsic safety, environmental benign and low cost. Layered molybdenum disulfide (MoS_2) is a potential cathode material for AZIBs. This study investigates the impact of manganese (Mn) doping on its electrochemical performance. Modifying the Mn doping ratio alters the MoS_2 structure, though X-ray diffraction confirms all samples show interlayer-expanded structure. Mn-MoS_2-20 shows a significantly improved specific capacity of 170 mAh/g at 0.1 A/g, exceeding that of undoped MoS_2. Furthermore, Mn doping enhances the rate performance of MoS2. While cycling stability at 0.5 A/g and 2 A/g improves with Mn doping, capacity still fades, indicating further improvements in structural stability are needed. This study shown that by doping an appropriate Mn level into MoS_2 structure would enhance the performance when applied as cathode material for AZIBs.

Key words - Aqueous Zinc-ion batteries; MoS_2; Mn doping; Rate performance stability

1. Introduction

Aqueous zinc-ion rechargeable batteries (AZIBs) are one of the most promising candidates for grid storage applications because of their safety, low cost, and the abundant of zinc resources [1–4]. One advantage of AZIBs is that they can use aqueous electrolytes. The ionic conductivity of aqueous electrolytes (up to 1 S/cm) is much higher than organic electrolytes (typically 1–10 mS/cm) [5]. Another advantage of AZIBs is the high capacity of the zinc anode (theoretical capacity 820 mAh/g), and the low redox potential of zinc (0.76 V vs. hydrogen reference electrode) [6–7]. However, the insertion/extraction reaction of Zn^{2+} is a two-electron process, resulting in a large ion migration energy barrier and high electrochemical polarization. Second, the insertion/extraction process easily collapse the microstructure and phase structure of cathode materials. These limitations limit the practical application of AZIBs. To overcome these limitations, the development, and research of potential cathode materials is of great importance.

So far, tunnel-structured and layered materials have been applied as cathodes for AZIBs, such as vanadium-based compounds, manganese-based oxides, organic compounds and molybdenum-based materials [4], [8]. MoS_2, with its layered structure and two-dimensional ion diffusion channels, is a promising candidate due to its high theoretical capacity (~320 mAh/g) and tunable phase and interlayer spacing [9]. However, its most stable form, 2H-MoS_2, is a semiconductor with small S-S interlayer spacing (~0.31 nm), hindering zinc-ion (0.55 nm) diffusion and limiting capacity and performance due to poor conductivity [10].

Scientists have explored various methods to improve the energy storage capacity and charge-discharge rates of MoS_2. For instance, metallic 1T-MoS_2 boasts better conductivity than its semiconducting 2H counterpart. While 1T-MoS_2 shows superior electrochemical performance, its limited zinc storage sites restrict its capacity due to strong electrostatic attraction between the framework and inserted Zn^{2+} ions, hindering further ion insertion [9]. Increasing interlayer spacing is a common approach to mitigate this interaction [10-11]. However, this weakens the van der Waals forces between MoS_2 layers, compromising structural stability [9]. Shuang Gao et al. synthesized 1T-MoS_2 with a 0.95 nm interlayer spacing (versus 0.62 nm for 2H-MoS_2), which when applied as cathode material delivered a high capacity of 226.2 mAh/g at 0.1 A/g, maintaining stability for roughly 500 cycles at 1 A/g [13]. To improve the performance of MoS_2 cathodes for AZIBs batteries and enable practical applications, we need to explore other strategies for enhancing their specific capacity and charge/discharge efficiency. Doping with heteroatoms or hybridizing with conductive subtracts can improve the electrical conductivity, structural stability, and defect density of MoS_2 materials [9, 11], but these strategies remain less studied.

In this study, we synthesized MoS_2 material doped with Mn atoms in different molar ratio by hydrothermal method and then studied the effect of this doping on the specific capacity and charge/discharge efficiency of MoS_2 when applied as a cathode for AZIBs. Mn was chosen because it is an abundant element, less toxic and less studied.

2. Experimental section

2.1. Materials

$Na_2MoO_4.2H_2O$ (99%, LOBA Chemie, India); Thiourea (99%), and hydrochloric acid (36-37%) (Xilong, China); $MnSO_4.H_2O$, N-Methyl-2-pyrrolidone (NMP), and Polyvinylidene difluoride (PVDF) (99%, Thermo Scientific); $Zn(CF_3SO_3)_2$ (98%, Macklin, China); Carbon black (Super P, Beyond batteries, Singapore); Glass fiber diaphragm (GF/B, Whatman); commercial Zn sheet (99.9%, 100 μm thick, Zhengzhou TCH Instrument,

China); 0.02 mm thick stainless steel current collector, Zhengzhou TCH Instrument, China). All chemicals used were of analytical grade.

First, 1.0 g of $Na_2MoO_4.2H_2O$ and 1.2 g of thiourea were dissolved in a mixed solvent containing 15 mL of water and 15 mL of ethanol. Then, 5 mL of HCl solution (2.0 M) was used to adjust the pH of the solution to about 1.0. Then, $MnSO_4.H_2O$ was added to the above solution and further stirred for 30 min. The hydrothermal reaction was carried out in a 100 mL teflon-lined stainless autoclave furnace, and heated at 180°C for 24 h. The final product was obtained by filtration, washing and drying as a black powder, and was designated as Mn-MoS_2-10. The amount of Mn doping in the sample could be tuned by changing the amount of $MnSO_4.H_2O$ precursor, and the obtained products were referred as Mn-MoS_2-5 and Mn-MoS_2-20, respectively. For comparison, the pristine MoS_2 sample was also synthesized under the same conditions but without adding the precursor $MnSO_4.H_2O$ (Table 1).

Table 1. *Stoichiometric ratios of precursors for the preparation of Mn-MoS_2*

Reaction precursor (mmol)			Mo: Mn	Name
Mo	Mn	S		
4.13	0.826	15.76	5:1	Mn-MoS_2-5
4.13	0.413	15.76	10:1	Mn-MoS_2-10
4.13	0.2605	15.76	20:1	Mn-MoS_2-20
4.13	0	15.76	-	Pristine MoS_2

2.2. Materials characterization

The crystal structure of the materials was determined by X-ray diffraction, using Cu K-α radiation with a wavelength of approximately λ of 1.54 Å (XRD, Bruker D8 Advance, Germany). The morphological features of the Mn-MoS_2 materials were performed using a scanning electron microscope (SEM, JSM-IT200, JEOL, Japan). The elemental composition was determined by energy dispersive X-ray spectroscopy (EDX). The characteristic vibrational properties of the Mn-MoS_2 materials were determined by a Raman system (LabRaman, Horiba Scientific) with a wavelength of λ=532 nm.

2.3. Galvanostatic charge-discharge measurement

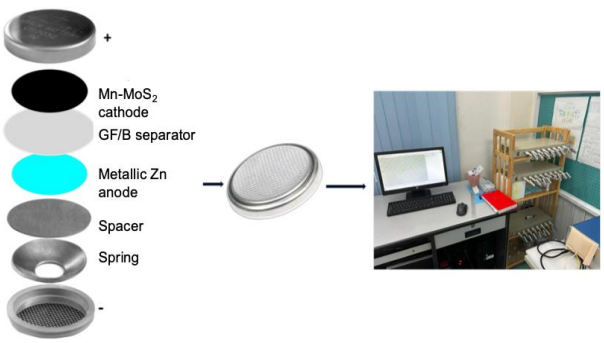

Figure 1. *Investigation of batteries charge-discharge performance using CR2032 coin cell*

Mn-MoS_2 cathode electrodes were prepared by mixing synthesized powder with Super-P carbon black and PVDF binder (7:2:1 mass ratio). N-methyl-2-pyrrolidone (NMP) solvent was added, and the mixture stirred for 6 hours to form a homogeneous slurry. This slurry was doctor bladed onto a stainless-steel current collector, vacuum-dried at 80°C for 12 hours, and cut into 12 mm diameter electrodes (~1–2 mg/cm² active material). Commercial zinc sheets (purity >99%), 12 mm in diameter, served as the anode. A Whatman GF/B glass fiber separator and 3M $Zn(CF_3SO_3)_2$ electrolyte completed the cell. These components were assembled into CR2032 coin cells (Figure 1) using a hydraulic press in air. Constant-current charge/discharge cycling was performed using a Land CT2001 battery cycler at room temperature (Figure 1).

3. Results and discussion

The crystal structures and phases of the synthesized Mn-MoS_2 materials were determined using X-ray diffraction method. Figure. 2 displays the X-ray diffraction patterns of Mn-MoS_2-5, Mn-MoS_2-10, Mn-MoS_2-20, and pristine MoS_2. All samples exhibited new diffraction peaks $(002)_{new}$ and (100) at approximately 9.27° and 18.45°, respectively. Calculated d-spacings (using Bragg's law: $n\lambda=2d\sin\theta$) were 9.53 Å and 4.80 Å, showing a new layered structure with a 9.53 Å interlayer spacing, exceeding the 6.15 Å spacing of 2H-MoS_2 (JCPDS 73-1508) [10, 12]. Compared to the pristine MoS_2, samples with manganese doping, besides the main peaks, appeared additional peaks consistent with the MnS phase [13-14]. This suggests that at these doping levels, manganese atoms both incorporate into the MoS_2 lattice and simultaneously react to form MnS phase [13].

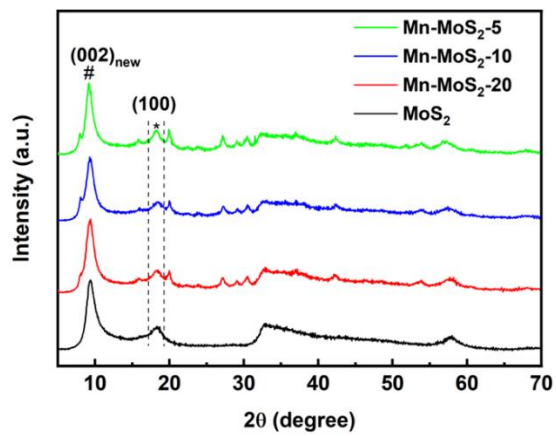

Figure 2. *X-ray diffraction patterns of as-synthesized Mn-MoS_2*

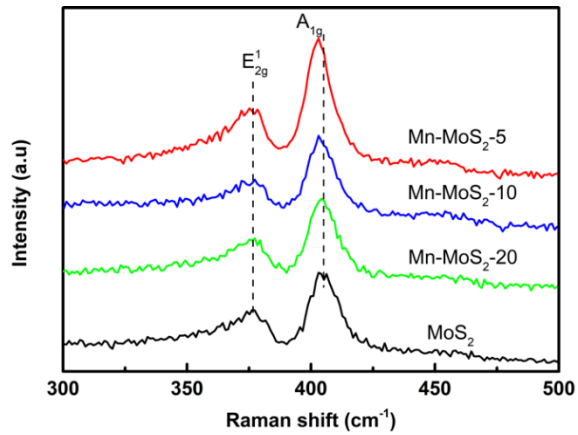

Figure 3. *Raman spectra of of as-synthesized Mn-MoS_2*

Raman spectroscopy was used to further elucidate the structures of the synthesized Mn-MoS_2 materials. As observed in Figure 3, all Mn-MoS_2 samples exhibited two characteristic peaks at around 376 and 403 cm^{-1}, corresponding to the E^1_{2g} in-plane of the two S and Mo atoms, and the A_{1g} out-plane of the S atoms vibrational modes of the typical layered structure of MoS_2 [9]. More interestingly, the blue shift of A_{1g} vibrational mode as the concentration of the Mn^{2+} precursor increased, while the vibrational peak E^1_{2g} remained unchanged. This can be explained by the distortion of the crystal lattice of MoS_2 because of the increased concentration of Mn doping atoms [16]. Furthermore, the distance between the two peaks gradually decreased as the concentration of the Mn^{2+} precursor increased, indicating that the increased concentration of the doping precursor reduced the number of MoS_2 layers [16].

The morphological features of the Mn-MoS_2 materials were observed using scanning electron microscopy (SEM).

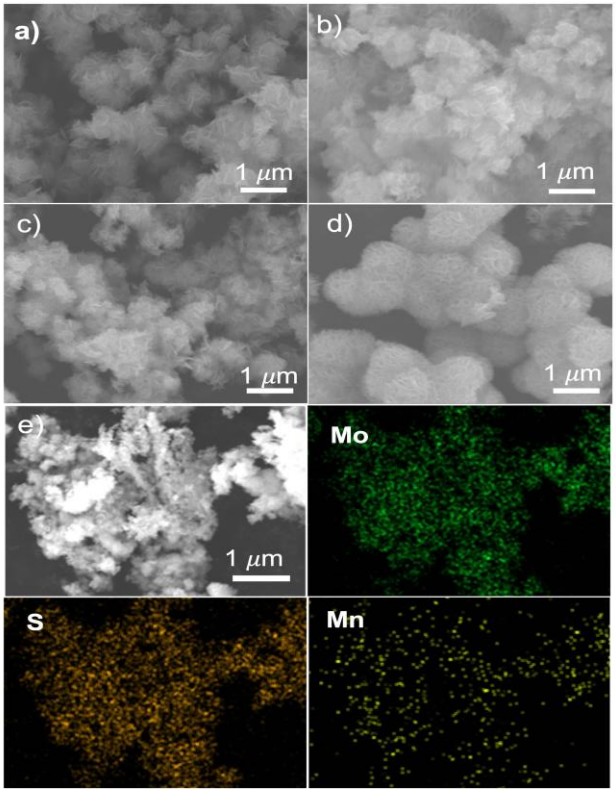

Figure 4. *SEM images of a) pristine MoS_2; b) Mn-MoS_2-20; c) Mn-MoS_2-10, và Mn-MoS_2-5, and representative EDX of Mn-MoS_2-10*

As shown in Figure 4a-d, the SEM images of all four synthesized Mn-MoS_2 samples showed a change in morphology from interwoven nanosheets to large-sized flower-like nanosheets with increasing Mn^{2+} content. This may be because Mn^{2+} ions promote the bonding of adjacent nanosheets during the growth of MoS_2 [17]. This morphology may be favorable for the diffusion of Zn^{2+} ions in the electrolyte solution. By using energy-dispersive X-ray spectroscopy, the existence of three main elements, Mo, S, Mn, and the uniform distribution of Mn doping atoms in the Mn-MoS_2-10 sample can be clearly identified (Figure 4e).

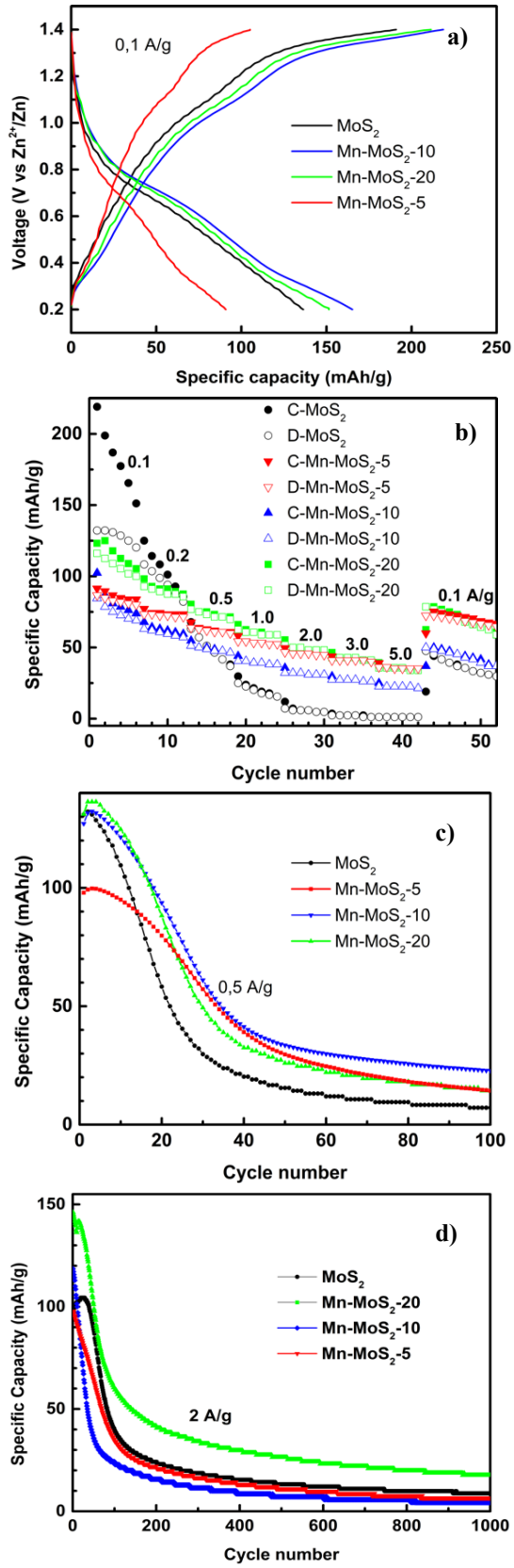

Figure 5. *Charge/discharge curves at 100 mA/g a); rate performance b); cycling performance at 0.5 A/g c); and 2 A/g d)*

The as-synthesized Mn-MoS_2 materials were used as cathodes for Zn-ion rechargeable batteries with aqueous electrolytes to evaluate the effect of Mn doping on the electrochemical properties. Figure 5a shows the

charge/discharge curves of the four material samples at a current density of 100 mA/g, and a potential window of 0.2-1.4 V (vs. Zn^{2+}/Zn). The Mn-MoS_2-20 material achieved a specific capacity of ~ 170 mAh/g, which was higher than that of Mn-MoS_2-10 (~ 150 mAh/g), pristine MoS_2 (~ 140 mAh/g), and MoS_2-5 (~ 95 mAh/g). The doping amount of Mn atoms clearly affected the MoS_2 material's specific capacity. Specifically, the specific capacity of MoS_2 materials is improved when the doping amount with Mn is low (Mn-MoS_2-20 and Mn-MoS_2-10), however, when the doping amount of Mn increases (Mn-MoS_2-5), the specific capacity decreases significantly. The specific capacity of Mn-MoS_2-20 materials in this study is equivalent to the specific capacity of MoS_2 materials doped with Fe atoms [11], and higher than that of published MoS_2 materials [12]. Figure 5b compares the charge/discharge performance at different rates of Mn-MoS_2 materials. For the original MoS_2 material, the specific capacity of the material decreases sharply when increasing the charge/discharge rate from 0.1 A/g to 5A/g, and at a rate of 5A/g the capacity of the material ~ 0 mAh/g. In contrast, all three materials when doped with Mn atoms at different ratios have more stable charge/discharge rate performance, and the specific capacities of these three materials decrease much more slowly when the charge/discharge rate increases from 0.1 to 5A/g. Manganese doping significantly improves the rate performance. To evaluate the materials' structural stability, we further evaluated their cycling performance at 0.5A/g and 2A/g. As shown in Figure 5c, at a cycling rate of 0.5A/g, the initial capacities of the materials all reached high values of ~ 100-150 mAh/g, and although the materials were more stable when doped with Mn atoms, the capacities of all four materials sharply decrease after 100 cycles. Similarly, at a high cycling rate of 2A/g, the Mn-MoS_2-20 material improved compared to the other three materials, but as at a cycling rate of 0.5 A/g, the specific capacities sharply decrease after 1000 cycles. Mn doping boosted the rate performance and stability of MoS_2, but its structural stability still needed improvement. These findings show that doping with heteroatom improves the rate capabilities of MoS_2, but structural stability requires further improvement for practical applications.

4. Conclusion

In summary, we synthesized Mn-MoS_2 materials by varying the amount of manganese precursor and investigated the influence of this doping on their electrochemical properties as AZIBs cathode materials. The interlayer-expanded structure is evident across all materials; Mn doping enhances the MoS_2 specific capacity, particularly improving rate performance at the appropriate Mn doping level. While doping with Mn atoms improves the cycling stability of MoS_2 materials, the specific capacity of all materials sharply decreased, indicating structural alterations in the structure of the materials during the charge/discharge process. These findings underscore the necessity for research that integrates Mn atom doping with structural stability to advance the stability and cycling performance of this prospective layered material.

Acknowledgments: This research is funded by the Ministry of Education and Training under the project number: B2023.DNA.06.

REFERENCES

[1] A. E. Blanc, D. Kundu, and L. F. Nazar, "Scientific challenges for the implementation of Zn-ion batteries", *Joule*, vol. 4, pp. 771-799, 2020.

[2] D. Kundu *et al*., "A high-capacity and long-life aqueous rechargeable zinc battery using a metal oxide intercalation cathode", *Nature Energy*, vol. 1, pp. 16119, 2016.

[3] Z. Liu *et al*., "Voltage issue of aqueous rechargeable metal-ion batteries", *Chemical Society Reviews*, vol. 49, pp. 180-232, 2020.

[4] L. Li *et al*., "Research progress on transition metal sulfide-based materials as cathode materials for Zn-ion batteries", *Journal of Energy Storage*, vol. 67, pp. 106714, 2023.

[5] D. Kundu *et al*., "A high capacity and long-life aqueous Zn battery using a metal oxide intercalation cathode", *Nature Energy*, vol. 1, pp. 16119, 2016.

[6] H. H. Yan *et al*., "Insights into the electrolyte strategy for aqueous Zn-ion batteries", *Coordination Chemistry Reviews*, vol. 452, pp. 214297, 2022.

[7] N. Zhang *et al*., "Rechargeable aqueous Zn–V_2O_5 battery with high energy density and long cycle life", *ACS Energy Letters*, vol. 3, pp. 1366-1372, 2018.

[8] Y. Li *et al*., "Designing advanced aqueous zinc-ion batteries: Principles, strategies, and perspectives", *Energy & Environmental Materials*, vol. 5, pp. 823-851, 2022.

[9] W. S. V. Lee *et al*., "Unraveling MoS_2 and transition metal dichalcogenides as functional zinc-ion batteries cathode: A perspective", *Small Methods*, vol. 5, pp. 1-14, 2021.

[10] H. Liang *et al.,* "Aqueous zinc-ion storage in MoS2 by tuning the intercalation energy", *Nano Letters*, vol. 19, pp. 3199-3206, 2019.

[11] J. Liu *et al*., "Fe doping 1T phase MoS_2 with enhanced Zn-ion storage ability and durability for high performance aqueous Zn-ion batteries", *Rare Metals*, vol. 44, pp. 253-263, 2025.

[12] C. Cai *et al*., "A nano interlayer spacing and rich defect 1T-MoS_2 as cathode for superior performance aqueous zinc-ion batteries", *Nanoscale Advances*, vol. 3, pp. 3780-3787, 2021.

[13] S. Gao *et al*., "Synthesis of 1T-MoS2 nanosheets with large space between layers for high-rate aqueous Zn-ion batteries", *Journal of Power Sources*, vol. 591, pp. 233866, 2024.

[14] L. Wang *et al*., "The universality applications of MoS_2@MnS heterojunction hollow microspheres for univalence organic or multivalence aqueous electrolyte energy storage device", *Journal of Power Sources*, vol. 518, pp. 230747, 2022.

[15] F. Chen *et al.,* "Novel design MnS-MoS_2 heterostructure for fast and stable Li/Na storage: Insights into the advanced mechanism attributed to phase engineering", *Advanced Functional Materials*, vol. 31, pp. 2007132, 2020.

[16] A. Azcatl *et al*., "Covalent nitrogen doping and compressive strain in MoS_2 by remote nitrogen plasma exposure", *Nano Letters*, vol. 16, pp. 5437-5443, 2016.

[17] K. Ma *et al*., "Multivalence-ion intercalation enables ultrahigh 1T phase MoS_2 nanoflowers to enhance sodium storage performance", *CCS Chemistry*, vol. 3, pp. 1472-1482, 2021.